A practical analysis of electron paramagnetic resonance spectra of rare earth ion pairs

2004 J. Phys.: Condens. Matter 16 R1

(http://iopscience.iop.org/0953-8984/16/3/R01)

INSTITUTE OF PHYSICS PUBLISHING JOURNAL OF PHYSICS: CONDENSED MATTER

J. Phys.: Condens. Matter **16** (2004) R1–R24 PII: S0953-8984(04)70068-5

TOPICAL REVIEW

A practical analysis of electron paramagnetic resonance spectra of rare earth ion pairs

O Guillot-Noël[1], Ph Goldner, P Higel and D Gourier

Ecole Nationale Supérieure de Chimie de Paris (ENSCP), Laboratoire de Chimie Appliquée de l'Etat Solide, UMR-CNRS 7574, 11 rue Pierre et Marie Curie, 75231 Paris Cedex 05, France

E-mail: guillotn@ext.jussieu.fr

Received 8 October 2003
Published 9 January 2004
Online at stacks.iop.org/JPhysCM/16/R1 (DOI: 10.1088/0953-8984/16/3/R01)

Abstract

The electron paramagnetic resonance (EPR) of rare earth ion pairs in solids is revisited. It is shown that the EPR pattern is very sensitive to the g factors of the paired ions. The two situations of ions characterized by identical g values and different g values are considered. To illustrate each case, some experimental EPR spectra are presented and analysed: the spectra of neodymium pairs in $LiYF_4$ and YVO_4 single crystals and ytterbium pairs in $CsCdBr_3$ (ions with identical g values) and the spectra of neodymium pairs in $SrAl_{12}O_{19}$ (ions with different g values).

Contents

[1] Author to whom any correspondence should be addressed.

1. Introduction

Research on materials doped with rare earth ion pairs or clusters is of fundamental interest for several applications. Recently, ytterbium pairs in the halide matrices $Cs_3Y_2Br_9$ [1], $Cs_3Lu_2Br_9$ [2] and $CsCdBr_3$ [3] have been suspected to be at the origin of an intrinsic optical bistability (IOB) observed for the near-infrared and the visible cooperative luminescence of Yb^{3+} ions [4]. Research on systems exhibiting IOB is motivated by the hope of replacing electrons by photons in future data systems. In the field of quantum information and quantum computing, a scheme for generating interacting quantum bits (qubits) in rare earth ion doped inorganic crystals has been recently proposed by Ohlsson *et al* [5]. The optical pumping procedure that has been developed in [5] is based on interacting rare earth ions. Coupling between rare earth ions, which play the role of qubits, is necessary to perform controlled logic.

For IOB and quantum computing applications, the key point is to synthesize rare earth doped crystals in which rare earth ions are arranged in pairs. A precise knowledge of ion–ion coupling mechanisms can help to better understand and to optimize the properties of both applications. Electron paramagnetic resonance (EPR) spectroscopy is a powerful tool to probe such ion–ion interactions in the ground state of a coupled paramagnetic system. Several experimental works have already been devoted in the past to the EPR study of rare earth–rare earth pair interactions in inorganic solids [6]. For example, magnetic interactions between Gd^{3+} ions in $LaCl_3$ [7] and $EuCl_3$ [8], between Ce^{3+} ions in $LaCl_3$ [9] and between Nd^{3+} ions in $LaCl_3$ [10, 11] and $LaBr_3$ [12] were studied by EPR a long time ago. Interactions between Gd^{3+} ions have also been measured in single crystals of $CsCdBr_3$ [13], $CsMgCl_3$, $CsMgBr_3$ [14], rare earth ethyl sulfate [15] and $YBa_2Cu_3O_6$ [16]. Yb^{3+} pairs and Tm^{3+} pairs have been found in alkaline fluorides [17, 18]. Yb^{3+} ion pairs have also been studied by EPR in $CsCdBr_3$ [19, 20] and $YAsO_4$ [21]. Several studies have also been devoted to neodymium pairs in $LiYF_4$, YVO_4 [22] and ethyl sulfate [23], cerium pairs in rare earth ethyl sulfate [24, 25], dysprosium pairs in rare earth ethyl sulfate [26], $KY(WO_4)_2$ [27], $[Dy(C_5H_4NCO_2)_3(H_2O)_2]_2$ (DyND) [28] and LaND [29] and erbium pairs in YPO_4, $YAsO_4$ [30], ErND [28] and LaND [29].

The aim of the present work is to revisit the problem of the EPR fingerprints of rare earth ion pairs by emphasizing the information we can obtain from such spectra, in particular in the situation where the two ions have slightly different g factors. As will be discussed in the next section, the two important interactions that are taken into account are the dipole–dipole magnetic interaction and the isotropic exchange interaction. From the dipole–dipole interaction, the rare earth pair orientation can be determined in the host, and the interionic distances between the two ions can be calculated. As Baker underlined in [6], it is more difficult to obtain information on the mechanisms responsible for the exchange interaction. However, different contributions can be extracted in some particular cases, as for example the direct exchange and the superexchange with its relationship to the rare earth–ligand covalency.

Two cases are discussed in this paper:

(i) pairs of similar ions characterized by the same ground state g value and
(ii) pairs of dissimilar ions characterized by different ground state g values where the ions involved in the pair can be identical or different.

It is well known that the EPR signature of a pair is composed of two transitions in case (i). The splitting between these two transitions is due to the dipole–dipole magnetic interaction and thus gives information on the orientation of the pairs in the structure and the ion–ion distances. The isotropic exchange interaction cannot be measured by EPR in this case. For case (ii), the EPR spectra are composed of four lines and the splitting between the lines depends on the dipole–dipole interaction as well as on the isotropic exchange interaction. In this case the EPR

study gives information on both interactions. Experimental spectra are given to illustrate each case. Case (i) will be illustrated by some of our previous works on neodymium pairs in $LiYF_4$ and YVO_4 single crystals [22], and the case of ytterbium pairs in $CsCdBr_3$ [20]. Case (ii) will be illustrated by neodymium pairs in the $SrAl_{12}O_{19}$ host. To our knowledge, this is only the second time that an EPR spectrum of identical rare earth ions with different g factors in their ground state has been presented. The first case corresponds to pairs of Dy^{3+} ions in dilute and semi-dilute LaND [29].

This paper is organized as follows. After having briefly presented in section 2 a bibliographic review of rare earth pair interactions in inorganic crystals, we discuss the two situations by an effective spin-Hamiltonian approach. Experimental EPR spectra are analysed in section 3 to illustrate the previous discussion.

2. Theoretical background: pairs of similar and dissimilar ions

The Hamiltonian of two coupled Kramers rare earth ions in neighbouring sites A and B can be written as

$$H = H^{\mathrm{A}} + H^{\mathrm{B}} + V^{\mathrm{AB}} \tag{1}$$

where H^{A} and H^{B} include the free-ion Hamiltonian (electron–electron and spin–orbit interaction terms) and the crystal field Hamiltonian. V^{AB} is the pairing interaction between the two ions. The free-ion Hamiltonian gives the $^{2S+1}\mathrm{L}_J$ multiplets separated by about 10^3–10^4 cm^{-1}. The crystal-field Hamiltonian removes the $2J+1$ degeneracy of the $^{2S+1}\mathrm{L}_J$ states into twofold degenerate states, referred to as Kramers doublets (KDs), separated by about 10–10^2 cm^{-1}. The residual degeneracy of the KD can only be lifted by a magnetic field. At liquid helium temperature, only the lowest KD is populated. Therefore, we can attribute to each Kramers ion an effective spin $S = 1/2$. The resulting effective spin Hamiltonian of the coupled Kramers ions under an external magnetic field $\mathbf{B}_0$ is thus

$$H_{\mathrm{pair}} = \beta \mathbf{B}_0 \cdot \tilde{g}^{\mathrm{A}} \cdot \mathbf{S}^{\mathrm{A}} + \beta \mathbf{B}_0 \cdot \tilde{g}^{\mathrm{B}} \cdot \mathbf{S}^{\mathrm{B}} + \mathbf{S}^{\mathrm{A}} \cdot \tilde{V} \cdot \mathbf{S}^{\mathrm{B}} \tag{2}$$

where β is the Bohr magneton and $\tilde{g}^{\mathrm{A}}$ and $\tilde{g}^{\mathrm{B}}$ are the g tensors associated with the ground state KD of ions A and B, respectively. The two ions of the pair can be dissimilar (different g factors) or similar (same g factor). For rare earth ions, four different mechanisms can participate in the interaction $\tilde{V}$ [6]: (i) the exchange interaction, which can originate from direct exchange and/or superexchange, (ii) the magnetic multipole interaction (MMI), (iii) the electric multipole interaction (EMI) and (iv) the virtual phonon exchange (VPE). For Kramers ions, the exchange and MMI interactions contribute to first order to the general interaction. The EMI interaction, for which the quadrupole–quadrupole interaction is predominant, and the VPE interaction contribute to second order through matrix elements with excited states [6]. As the aim of this paper is to derive the precise EPR signature of Kramers ion pairs, we will not consider the EMI and VPE interactions in the following discussion. These interactions do not change the shape of the EPR spectrum but rather induce small shifts in the EPR lines, equivalent to small shifts in the g value compared to isolated ions. Moreover, concerning the magnetic multipole expansion, the magnetic dipole–dipole (MDD) interaction is the predominant term. The next term in the magnetic multipole interaction, the dipole–octupole interaction, is smaller than the MDD term by a factor $\langle r^2 \rangle / R^2$, where r is the electron–nucleus distance and R the distance between rare earth ions [6]. If we take the value of $\langle r^2 \rangle$ tabulated by Freeman and Watson in [31], for the Ce^{3+} ion (the biggest rare earth ion) $\langle r^2 \rangle = 0.3358$ Å^2 and for a very common distance R of 4 Å, we find $\langle r^2 \rangle / R^2 = 0.02$. Thus, the dipole–octupole interaction contributes only a few per cent to the magnetic multipole expansion. If we retain the most important terms,

the V^{AB} interaction can be written as follows in the effective spin Hamiltonian:

$$\begin{aligned} V^{AB} &= \mathbf{S}^A \cdot \tilde{V} \cdot \mathbf{S}^B \\ &= \mathbf{S}^A \cdot \tilde{J}^{AB}_{exch} \cdot \mathbf{S}^B + \mathbf{S}^A \cdot \tilde{D}^{AB}_{dd} \cdot \mathbf{S}^B \end{aligned} \tag{3}$$

where $\tilde{J}^{AB}_{exch}$ is the exchange contribution and $\tilde{D}^{AB}_{dd}$ the magnetic dipole–dipole contribution. $\tilde{D}^{AB}_{dd}$ has the following well known expression [32]:

$$\tilde{D}^{AB}_{dd} = \frac{\boldsymbol{\mu}^A \cdot \boldsymbol{\mu}^B}{R^3} - \frac{3(\boldsymbol{\mu}^A \cdot \mathbf{R})(\boldsymbol{\mu}^B \cdot \mathbf{R})}{R^5} \tag{4}$$

where $\boldsymbol{\mu}^A$ and $\boldsymbol{\mu}^B$ are the magnetic dipole moments written as $\boldsymbol{\mu}^{A,B} = \beta \tilde{g}^{A,B} \cdot \mathbf{S}^{A,B}$. This interaction allows us to retrieve the pair orientation and to calculate the distance R between the two ions.

The exchange interaction can be factorized into an isotropic part (Heisenberg type) and a traceless anisotropic part so that

$$\mathbf{S}^A \cdot \tilde{J}^{AB}_{exch} \cdot \mathbf{S}^B = -2J\mathbf{S}^A \cdot \mathbf{S}^B + \mathbf{S}^A \cdot \tilde{J}' \cdot \mathbf{S}^B \tag{5}$$

where $\mathrm{Tr}\,\tilde{J}' = 0$ and $3(-2J) = \mathrm{Tr}\,\tilde{J}^{AB}_{exch}$.

Table 1 gathers some values of pair interactions found in the literature with the dipole–dipole magnetic interaction represented by the component $D_{zz} = -2g^2_{zz}\frac{\beta^2}{R^3}$ of the $\tilde{D}^{AB}_{dd}$ tensor, the isotropic exchange interaction $(-2J)$ and the J'_{zz} component of the anisotropic exchange term $\tilde{J}'$. In many cases encountered in the rare earth literature, the EPR pair spectrum is perfectly explained by taking into account only the isotropic exchange term $-2J\mathbf{S}^A \cdot \mathbf{S}^B$ and the magnetic dipole–dipole term $\mathbf{S}^A \cdot \tilde{D}^{AB}_{dd} \cdot \mathbf{S}^B$ (table 1). This is the case for Yb–Yb and some Tm–Tm pairs in SrF_2, all the rare earth pairs in the $CsCdBr_3$ host, Gd–Gd pairs in $CsMgBr_3$, $CsMgCl_3$, $LaCl_3$, $EuCl_3$ and lanthanum ethyl sulfate (LaES), Dy–Dy pairs in DyES and Gd–Ce pairs in CeES. The Dy–Dy pairs and Er–Er pairs in lanthanide nicotinade dihydrate (DyND, ErND and LaND) are characterized by a purely magnetic dipole–dipole interaction. In some other cases, the anisotropic part of the exchange interaction ($\mathbf{S}^A \cdot \tilde{J}' \cdot \mathbf{S}^B$) contributes to second order to the pair interaction (table 1): this is the case of Nd–Nd and Gd–Nd pairs in lanthanum ethyl sulfate (LaES), Nd–Nd pairs in NdES, Gd–Dy pairs in DyES, Gd–Gd pairs in $YBa_2Cu_3O_6$, Er–Er pairs in YPO_4 and $YAsO_4$ and some Dy–Dy pairs in $KY(WO_4)_2$. In a few cases, the anisotropic exchange contribution can be of the same order of magnitude or even larger than the isotropic exchange term and the magnetic dipole–dipole term: this is the case for Tm–Tm pairs in SrF_2, CaF_2 and BaF_2, Nd–Nd pairs in $LaCl_3$ and $LaBr_3$, Nd–Nd pairs in $NdCl_3$, Gd–Gd pairs in $LaCl_3$ and $EuCl_3$ and some Dy–Dy pairs in $KY(WO_4)_2$. In most of the cases described in table 1, the shorter the distance the higher is the contribution of the exchange terms (isotropic and anisotropic). If the exchange interaction is a direct exchange interaction, this term rapidly decreases with ion–ion distances, and for distances above 5 Å the contribution of the anisotropic part of the exchange can be neglected.

In conclusion, the procedure for the study of EPR pair spectra of Kramers ions can be summarized as follows.

(i) The spectrum is analysed by considering the following Hamiltonian where only the isotropic exchange interaction and the magnetic dipole–dipole interaction are considered:

$$H_{pair} = \beta\mathbf{B}_0 \cdot \tilde{g}^A \cdot \mathbf{S}^A + \beta\mathbf{B}_0 \cdot \tilde{g}^B \cdot \mathbf{S}^B - 2J\mathbf{S}^A \cdot \mathbf{S}^B + \mathbf{S}^A \cdot \tilde{D}^{AB}_{dd} \cdot \mathbf{S}^B. \tag{6}$$

(ii) If discrepancies are found between the experimental spectrum and the calculated spectrum, one has to add the contribution of the anisotropic exchange interaction $\mathbf{S}^A \cdot \tilde{J}' \cdot \mathbf{S}^B$ to equation (6).

Table 1. Parameters of rare earth pairs in different matrices. The dipole–dipole interaction (D_{zz} component), the isotropic interaction ($-2J$) and the anisotropic exchange term (J'_{zz} component) are gathered. The ion–ion distances and the g factor are indicated. (\ means not given or not measured.)

Host	Pair	R (Å)	g factor	$\mathbf{D}_{zz}$ (cm^{-1})	$-2J$ (cm^{-1})	$\mathbf{J}'_{zz}$ (cm^{-1})	References
SrF_2	Yb–Yb	10	$g_\parallel = 2.813$ $g_\perp = 3.746$	−0.0069	0.012 2	0	[17]
	Tm–Tm	4.09	$g_{xx} = 3.448$ $g_{yy} = 3.383$ $g_{zz} = 2.512$	−0.0799	−0.032 1	0.019 2	[18]
	Tm–Tm	5.78	$g_\parallel = 3.4208$ $g_\perp = 3.4448$	−0.0525	0	0	[18]
$CsCdBr_3$	Yb–Yb	5.88	$g_\parallel = 2.503$ $g_\perp = 2.619$	−0.0267	−0.003 2	0	[20]
	Gd–Gd	6	$g = 1.991$	−0.0159	0.000 68	0	[13]
	Nd–Nd	5.918	$g_\parallel = 3.3$ $g_\perp = 0$	−0.0455	0.002 33	0	[33]
	Tm–Tm	5.943	$g = 12.30$	−0.6243	0	0	[34]
$CsMgBr_3$	Gd–Gd	5.89	$g = 1.991$	−0.0168	0.000 8	0	[14]
$CsMgCl_3$	Gd–Gd	5.40	$g = 1.991$	−0.0218	0.001 07	0	[14]
$LaCl_3$	Gd–Gd	4.375	$g = 1.991$	−0.0410	0.013 30	0	[7]
	Gd–Gd	4.843	$g = 1.991$	−0.0302	−0.059 5	0	[7]
$EuCl_3$	Gd–Gd	4.133	$g = 1.997$	−0.0489	0.048 8	0	[8]
	Gd–Gd	4.730	$g = 1.997$	−0.0326	−0.063 68	0	[8]
LaES	Nd–Nd	7.08	$g_\parallel = 3.552$ $g_\perp = 2.062$	−0.0308	\	0.004 2	[6]
	Gd–Nd	7.08	$g^{Gd} = 1.991$ $g_\parallel^{Nd} = 3.535$ $g_\perp^{Nd} = 2.072$	−0.0172	\	0.000 7	[6]
	Gd–Gd	7.11	$g = 1.991$	−0.0096	0.000 2	0	[6]
NdES	Nd–Nd	7.07	$g_\parallel = 3.60$ $g_\perp = 2.072$	−0.0318	\	0.003 1	[23]
DyES	Gd–Dy	7.04	$g^{Gd} = 1.991$ $g_\parallel^{Dy} = 10.94$ $g_\perp^{Dy} = 0$	−0.0541	\	−0.001 4	[6]
	Dy–Dy	7.04	$g_\parallel^{Dy} = 10.94$ $g_\perp^{Dy} = 0$	−0.2971	0	0	[24]
CeES	Gd–Ce	7.11	$g^{Gd} = 1.991$ $g_\parallel^{Ce} = 3.76$ $g_\perp^{Ce} = 0$	−0.0180	\	0	[6]
$YBa_2Cu_3O_6$	Gd–Gd	3.8586	$g = 1.9871$	−0.0595	0.108 4	0.006	[16]
CaF_2	Tm–Tm	3.85	$g_{xx} = 3.451$ $g_{yy} = 3.58$ $g_{zz} = 3.385$	−0.1739	−0.088 5	0.024 6	[18]
	Tm–Tm	5.44	$g_\parallel = 3.427$ $g_\perp = 3.455$	−0.0632	−0.003 4	0.017 6	[18]
BaF_2	Tm–Tm	4.37	$g_{xx} = 3.436$ $g_{yy} = 3.436$ $g_{zz} = 3.654$	−0.1386	0.013 4	0.022	[18]
YPO_4	Er–Er	3.671	$g_\parallel = 6.48$ $g_\perp = 4.8$	−0.7352	\	0.023	[30]

Table 1. (Continued.)

Host	Pair	R (Å)	g factor	$\mathbf{D}_{zz}$ (cm^{-1})	$-2J$ (cm^{-1})	$\mathbf{J}'_{zz}$ (cm^{-1})	References
$YAsO_4$	Er–Er	3.845	$g_\parallel = 6.639$ $g_\perp = 5.177$	−0.6716	\	−0.011	[30]
YVO_4	Er–Er	3.88	$g_\parallel = 3.561$ $g_\perp = 7.017$	−0.1880	\	−0.092	[30]
$KY(WO_4)_2$	Dy–Dy	4.06	$g_{xx} = 3.436$ $g_{yy} = 3.436$ $g_{zz} = 3.654$	−0.1728	0.269 9	0.530 8	[27]
	Dy–Dy	7.53	idem	−0.0271	−0.017 1	−0.033 5	[27]
	Dy–Dy	8.81	idem	−0.0169	0.008 1	0.015 9	[27]
DyND	Dy–Dy	4.37	$g_{xx} = 0$ $g_{yy} = 0$ $g_{zz} = 17.8$	−3.28	0	0	[28]
LaND	Dy-Dy	4.22–4.37	$g^{\mathrm{A}}_{xx} = g^{\mathrm{B}}_{xx} = 0$ $g^{\mathrm{A}}_{yy} = g^{\mathrm{B}}_{yy} = 0$ $g^{\mathrm{A}}_{zz} = 17.61$ $g^{\mathrm{B}}_{zz} = 17.8$	−3.613 to −3.253	0	0	[29]
$LaCl_3$	Nd–Nd	4.37	$g_\parallel = 4.018$ $g_\perp = 1.710$	−0.1676	\	0.546	[6, 12]
$NdCl_3$	Nd–Nd	4.23	$g_\parallel = 4.018$ $g_\perp = 1.710$	−0.1848	0.53	1.09	[6, 35]
$LaBr_3$	Nd–Nd	4.50	$g_\parallel = 1.843$ $g_\perp = 3.924$	−0.1413	\	0.675	[6, 12]

(iii) If discrepancies are still present, one has to consider the second order effects of the electric multipole interaction (mainly quadrupole–quadrupole interaction) and the virtual phonon exchange.

In the following discussion concerning the different types of EPR pair spectrum that can be encountered, we will only consider the Hamiltonian of equation (6) as the other terms do not modify the shape of the spectrum.

Two cases have to be taken into account:

(i) the two ions of the pair are similar with exactly the same g values $\tilde{g}^{\mathrm{A}} = \tilde{g}^{\mathrm{B}}$ and
(ii) the two ions of the pair are dissimilar with different g values $\tilde{g}^{\mathrm{A}} \neq \tilde{g}^{\mathrm{B}}$, which can be encountered either for the same ions in crystallographically different sites, or for two different ions.

2.1. Pairs of ions with the same g values

In the case of identical ions, the spin Hamiltonian of the pair is that of equation (6) with $\tilde{g}^{\mathrm{A}} = \tilde{g}^{\mathrm{B}} = \tilde{g}$. This situation is encountered in a host with only one substitution site without charge compensation. In the following, we will take the z quantification axis parallel to the pair axis. We will consider that the reference axis set (x, y, z) is the principal axis of the g tensor:

$$\tilde{g} = \begin{pmatrix} g_{xx} & 0 & 0 \\ 0 & g_{yy} & 0 \\ 0 & 0 & g_{zz} \end{pmatrix},$$

with $g_{xx} \neq g_{yy} \neq g_{zz}$ in the case of an orthorhombic g tensor, $g_{xx} = g_{yy} = g_\perp$ and $g_{zz} = g_\parallel$ for an axial g tensor and $g_{xx} = g_{yy} = g_{zz} = g$ for an isotropic g tensor. In

the individual effective spin $\{|M_S^{\mathrm{A}}, M_S^{\mathrm{B}}\rangle\}$ representation, each state can be described by the z components $M_S^{\mathrm{A}} = \pm\frac{1}{2}$ and $M_S^{\mathrm{B}} = \pm\frac{1}{2}$ of the effective spins $\mathbf{S}^{\mathrm{A}}$ and $\mathbf{S}^{\mathrm{B}}$. When the external magnetic field $\mathbf{B}_0$ is parallel to the pair axis z, H^z_{pair} is written as follows in the basis set $\{|\varphi_1\rangle = |-,-\rangle; |\varphi_2\rangle = \frac{1}{\sqrt{2}}(|+,-\rangle - |-,+\rangle); |\varphi_3\rangle = \frac{1}{\sqrt{2}}(|+,-\rangle + |-,+\rangle); |\varphi_4\rangle = |+,+\rangle\}$:

$$H^z_{\mathrm{pair}} = \begin{pmatrix} -g_{zz}\beta B_0 - \frac{J}{2} - D_1^z & 0 & 0 & D_4 \\ 0 & \frac{3J}{2} + D_2 & 0 & 0 \\ 0 & 0 & -\frac{J}{2} + D_3 & 0 \\ D_4 & 0 & 0 & g_{zz}\beta B_0 - \frac{J}{2} - D_1^z \end{pmatrix} \tag{7}$$

with $D_1^z = \frac{\beta^2}{2R^3} g_{zz}^2$, $D_2 = \frac{\beta^2}{2R^3}(g_{zz}^2 - \frac{g_{xx}^2}{2} - \frac{g_{yy}^2}{2})$, $D_3 = \frac{\beta^2}{2R^3}(g_{zz}^2 + \frac{g_{xx}^2}{2} + \frac{g_{yy}^2}{2})$ and $D_4 = \frac{\beta^2}{4R^3}(g_{xx}^2 - g_{yy}^2)$. The diagonalization of the above matrix (equation (7)) gives the following eigenvalues and eigenvectors for H^z_{pair}:

$$\begin{aligned} E_1^z &= -\frac{J}{2} - D_1^z - \Delta; & |\Psi_1^z\rangle &= \alpha|-,-\rangle + \beta|+,+\rangle \\ E_2^z &= +\frac{3J}{2} + D_2; & |\Psi_2^z\rangle &= \frac{1}{\sqrt{2}}(|+,-\rangle - |-,+\rangle) \\ E_3^z &= -\frac{J}{2} + D_3; & |\Psi_3^z\rangle &= \frac{1}{\sqrt{2}}(|+,-\rangle + |-,+\rangle) \\ E_4^z &= -\frac{J}{2} - D_1^z + \Delta; & |\Psi_4^z\rangle &= -\beta|-,-\rangle + \alpha|+,+\rangle \end{aligned} \tag{8}$$

with $|\alpha|^2 + |\beta|^2 = 1$ and $\Delta = \sqrt{D_4^2 + g_{zz}^2\beta^2 B_0^2}$. Coefficients α and β are given in the appendix.

The isotropic exchange term splits the fourfold degenerate pair ground state $\{|\Psi_1^z\rangle; |\Psi_2^z\rangle, |\Psi_3^z\rangle; |\Psi_4^z\rangle\}$ into a singlet $|\Psi_2^z\rangle = |\varphi_2\rangle = \frac{1}{\sqrt{2}}(|+,-\rangle - |-,+\rangle)$ at energy $\frac{3J}{2}$ and a triplet $\{|\Psi_1^z\rangle; |\Psi_3^z\rangle; |\Psi_4^z\rangle\}$ at energy $-\frac{J}{2}$. The dipolar interaction and the Zeeman term shifts the singlet state $|\Psi_2^z\rangle$ by $+D_2$ and splits the triplet state into three singlet states: $|\Psi_1^z\rangle$ at energy $-\frac{J}{2} - D_1^z - \Delta$, $|\Psi_3^z\rangle$ at energy $-\frac{J}{2} + D_3$ and $|\Psi_4^z\rangle$ at energy $-\frac{J}{2} - D_1^z + \Delta$. The resulting energy level diagram is shown figure 1(a).

In standard EPR experiments, the external oscillating magnetic field $\mathbf{B}_1$ which induces the transitions is linearly polarized perpendicular to the static magnetic field $\mathbf{B}_0$, along the x axis for example. The transition probability P_{if}^z between two states $|i\rangle$ and $|f\rangle$ is proportional to the square of the matrix element $|\langle f|g_{xx}S_x|i\rangle|^2$, which gives

$$P_{if}^z \propto \begin{pmatrix} 0 & 0 & (\alpha+\beta)^2 & 0 \\ 0 & 0 & 0 & 0 \\ (\alpha+\beta)^2 & 0 & 0 & (\alpha-\beta)^2 \\ 0 & 0 & (\alpha-\beta)^2 & 0 \end{pmatrix} \tag{9}$$

written in the order $\{|\Psi_1^z\rangle; |\Psi_2^z\rangle, |\Psi_3^z\rangle; |\Psi_4^z\rangle\}$. For two identical ions and when $\mathbf{B}_0$ is parallel to the pair axis, the EPR pair spectrum is composed of two lines which are symmetrically placed around Δ at energies $\Delta \pm D$ with $D = D_1^z + D_3 = \frac{\beta^2}{2R^3}(2g_{zz}^2 + \frac{g_{xx}^2}{2} + \frac{g_{yy}^2}{2})$ and with intensities proportional to $(\alpha \pm \beta)^2$ (equation (9)).

When the external magnetic field $\mathbf{B}_0$ is perpendicular to the z pair axis, the x axis for example, H^x_{pair} in the $\{|\varphi_1\rangle; |\varphi_2\rangle; |\varphi_3\rangle; |\varphi_4\rangle\}$ basis state is

$$H^x_{\mathrm{pair}} = \begin{pmatrix} -\frac{J}{2} - D_1^z & 0 & \frac{g_{xx}}{\sqrt{2}}\beta B_0 & D_4 \\ 0 & \frac{3J}{2} + D_2 & 0 & 0 \\ \frac{g_{xx}}{\sqrt{2}}\beta B_0 & 0 & -\frac{J}{2} + D_3 & \frac{g_{xx}}{\sqrt{2}}\beta B_0 \\ D_4 & 0 & \frac{g_{xx}}{\sqrt{2}}\beta B_0 & -\frac{J}{2} - D_1^z \end{pmatrix} \tag{10}$$

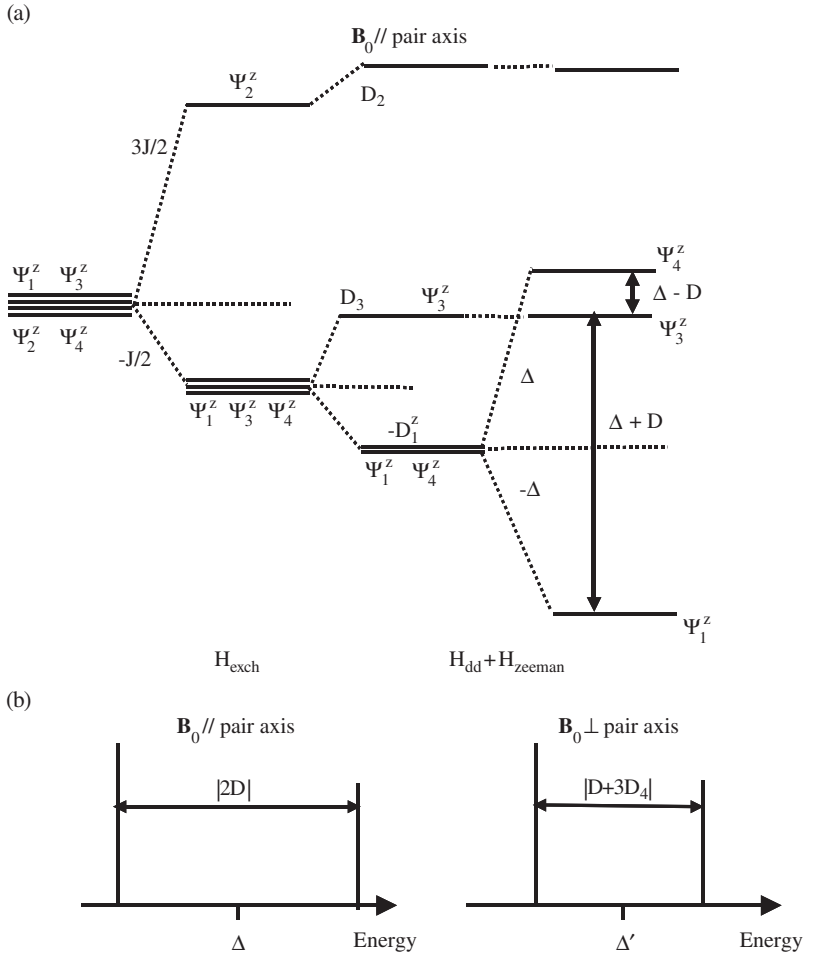

Figure 1. (a) Energy level diagram of a pair of identical Kramers ions ($\tilde{g}^{\mathrm{A}} = \tilde{g}^{\mathrm{B}} = \tilde{g}$) for a fixed value of the external magnetic field $\mathbf{B}_0$ parallel to the pair axis. The g factor is orthorhombic: $g_{xx} \neq g_{yy} \neq g_{zz}$. For the diagram, J is positive and $\Delta > D_1^z + D_3$. The two allowed EPR transitions are represented by arrows. (b) Schematic EPR spectrum for identical ions with $\mathbf{B}_0$ parallel and perpendicular to the pair axis.

which gives after diagonalization

$$
\begin{aligned}
E_1^x &= -\frac{J}{2} + \frac{D_1^x}{2} + \Delta'; \qquad & |\Psi_1^x\rangle &= \alpha'(|-,-\rangle + |+,+\rangle) + \beta'\left(\frac{|-,+\rangle + |+,-\rangle}{\sqrt{2}}\right) \\
E_2^x &= -\frac{J}{2} + \frac{D_1^x}{2} - \Delta'; \qquad & |\Psi_2^x\rangle &= \gamma'(|-,-\rangle + |+,+\rangle) + \delta'\left(\frac{|-,+\rangle + |+,-\rangle}{\sqrt{2}}\right) \\
E_3^x &= +\frac{3J}{2} + D_2; \qquad & |\Psi_3^x\rangle &= \frac{1}{\sqrt{2}}(|+,-\rangle - |-,+\rangle) \\
E_4^x &= -\frac{J}{2} - (D_1^z + D_4); \qquad & |\Psi_4^x\rangle &= \frac{1}{\sqrt{2}}(-|-,-\rangle + |+,+\rangle)
\end{aligned}
\tag{11}
$$

with $|\alpha'|^2 + |\beta'|^2 = 0.5$, $|\gamma'|^2 + |\delta'|^2 = 0.5$, $\Delta' = \frac{1}{2}\sqrt{(D_1^z - D_4 + D_3)^2 + 4g_{xx}^2\beta^2 B_0^2}$ and $D_1^x = \frac{\beta^2}{2R^3}g_{xx}^2$. Coefficients α', β', γ' and δ' are given in the appendix.

In this orientation, the transition probability P_{if}^{x} is proportional to the square of the matrix element $|\langle f|g_{zz}S_z|i\rangle|^2$:

$$P_{if}^{x} \propto \begin{pmatrix} 0 & 0 & 0 & \alpha'^2 \\ 0 & 0 & 0 & \gamma'^2 \\ 0 & 0 & 0 & 0 \\ \alpha'^2 & \gamma'^2 & 0 & 0 \end{pmatrix} \tag{12}$$

in the $\{|\Psi_1^x\rangle; |\Psi_2^x\rangle, |\Psi_3^x\rangle; |\Psi_4^{xx}\rangle\}$ basis set.

When $\mathbf{B}_0$ is perpendicular to the pair axis, the EPR pair spectrum is thus composed of two lines which are symmetrically placed around Δ' at energies $|\Delta' \pm (\frac{3D_4}{2} + \frac{D}{2})|$ with intensities proportional to α'^2 and γ'^2, respectively (equation (12)).

Figure 1(b) gathers the two expected EPR pair spectra when $\mathbf{B}_0$ is parallel and perpendicular to the pair axis. We obtain a direct measurement of the distance R between the two ions and the orientation of the pair in the structure by measuring the splitting between the two lines as a function of the orientation of the magnetic field. In the case of a orthorhombic g factor, this splitting is D for B_0 parallel to the pair axis and $(\frac{3D_4}{2} + \frac{D}{2})$ for B_0 perpendicular to the pair axis. When the g factor is axial or isotropic ($D_4 = 0$), the splitting between the two lines for the field parallel to the pair axis is twice that measured with the magnetic field perpendicular to the pair axis: $D = \frac{\beta^2}{2R^3}(2g_\parallel^2 + g_\perp^2)$ for an axial site and $D = \frac{\beta^2}{2R^3}(3g^2)$ for an isotropic site. This very simple behaviour indicates that we are dealing with axial or isotropic g tensor for the ions of the pair. Departure from this rule indicates an orthorhombic g factor with a non-zero D_4 term.

When the two ions are identical, the only allowed EPR transitions are between the wavefunctions of the triplet state (equations (9) and (12)). Therefore, it is not possible to measure the isotropic exchange J term from the EPR pattern. The only two possibilities to measure the exchange term are

(i) when J is high enough to be measured by high resolution optical spectroscopies (absorption and emission) [22], and
(ii) when the two ions have isotopes with non-zero nuclear spins giving a hyperfine structure, which is also split by the pair interactions [20, 36]. These two situations are illustrated in section 3.

2.2. Pairs of ions with different g values

The case of ion pairs with different g factors corresponds to the spin Hamiltonian of equation (6). This situation can be encountered in a host with different substitution sites and when a charge compensation defect is close to one of the ions of the pair. As in the preceding case, we consider that the pair axis is parallel to the z quantification axis. Moreover, we assume that the two different g tensors have the same orientation of their principal axes. This hypothesis implies that the site symmetries of the two ions involved in the pairs have the same orientation. In the more general case, an equivalent treatment can be applied and the shape of the spectrum is the same. When the external magnetic field $\mathbf{B}_0$ is parallel to the pair axis, the pair Hamiltonian H_{pair}^{z} is written as follows in the basis set $\{|\varphi_1\rangle; |\varphi_2\rangle; |\varphi_3\rangle; |\varphi_4\rangle\}$:

$$H_{\text{pair}}^{z} = \begin{pmatrix} -\frac{g_{zz}^{\text{A}}+g_{zz}^{\text{B}}}{2}\beta B_0 - \frac{J}{2} - D_1^z & 0 & 0 & D_4 \\ 0 & \frac{3J}{2} + D_2 & \frac{g_{zz}^{\text{A}}-g_{zz}^{\text{B}}}{2}\beta B_0 & 0 \\ 0 & \frac{g_{zz}^{\text{A}}-g_{zz}^{\text{B}}}{2}\beta B_0 & -\frac{J}{2} + D_3 & 0 \\ D_4 & 0 & 0 & \frac{g_{zz}^{\text{A}}+g_{zz}^{\text{B}}}{2}\beta B_0 - \frac{J}{2} - D_1^z \end{pmatrix} \tag{13}$$

Table 2. Energies and intensities of the four-line EPR pair spectrum of dissimilar ions with the external magnetic field parallel to the pair axis.

Transition	Energy	Intensity proportionnal to
$E_1^z \to E_2^z$	$\lvert 2D_1^z + J + (\Delta_1^z - \Delta_2^z)\rvert$	$[c(g_{xx}^{\mathrm{A}} - g_{xx}^{\mathrm{B}})(a-b) + d(g_{xx}^{\mathrm{A}} + g_{xx}^{\mathrm{B}})(a+b)]^2$
$E_1^z \to E_3^z$	$\lvert 2D_1^z + J + (\Delta_1^z + \Delta_2^z)\rvert$	$[-d(g_{xx}^{\mathrm{A}} - g_{xx}^{\mathrm{B}})(a-b) + c(g_{xx}^{\mathrm{A}} + g_{xx}^{\mathrm{B}})(a+b)]^2$
$E_4^z \to E_2^z$	$\lvert -2D_1^z - J + (\Delta_1^z + \Delta_2^z)\rvert$	$[-c(g_{xx}^{\mathrm{A}} - g_{xx}^{\mathrm{B}})(a+b) + d(g_{xx}^{\mathrm{A}} + g_{xx}^{\mathrm{B}})(a-b)]^2$
$E_4^z \to E_3^z$	$\lvert -2D_1^z - J + (\Delta_1^z - \Delta_2^z)\rvert$	$[d(g_{xx}^{\mathrm{A}} - g_{xx}^{\mathrm{B}})(a+b) + c(g_{xx}^{\mathrm{A}} + g_{xx}^{\mathrm{B}})(a-b)]^2$

with $D_1^z = \frac{\beta^2}{2R^3} g_{zz}^{\mathrm{A}} g_{zz}^{\mathrm{B}}$, $D_2 = \frac{\beta^2}{2R^3}(g_{zz}^{\mathrm{A}} g_{zz}^{\mathrm{B}} - \frac{g_{xx}^{\mathrm{A}} g_{xx}^{\mathrm{B}}}{2} - \frac{g_{yy}^{\mathrm{A}} g_{yy}^{\mathrm{B}}}{2})$ and $D_3 = \frac{\beta^2}{2R^3}(g_{zz}^{\mathrm{A}} g_{zz}^{\mathrm{B}} + \frac{g_{xx}^{\mathrm{A}} g_{xx}^{\mathrm{B}}}{2} + \frac{g_{yy}^{\mathrm{A}} g_{yy}^{\mathrm{B}}}{2})$ and $D_4 = \frac{\beta^2}{4R^3}(g_{xx}^{\mathrm{A}} g_{xx}^{\mathrm{B}} - g_{yy}^{\mathrm{A}} g_{yy}^{\mathrm{B}})$. The off-diagonal term $\frac{g_{zz}^{\mathrm{A}} - g_{zz}^{\mathrm{B}}}{2}\beta B_0$ of equation (13) mixes the singlet state $|\varphi_2\rangle$ with the levels $|\varphi_3\rangle$ of the triplet state. This mixing allows EPR transitions between the triplet and the singlet states, in contrast to the case of identical ions where only transitions within the triplet states are allowed. We thus expect four transitions in the EPR spectra when $g^{\mathrm{A}} - g^{\mathrm{B}} \neq 0$.

The diagonalization of the matrix (equation (13)) gives the following eigenvalues and eigenvectors:

$$\begin{aligned}
E_1^z &= -\frac{J}{2} - D_1^z - \Delta_1^z; \qquad & |\Psi_1^z\rangle &= a|-,-\rangle + b|+,+\rangle \\
E_2^z &= +\frac{J}{2} + D_1^z - \Delta_2^z; \qquad & |\Psi_2^z\rangle &= c\left(\frac{|+,-\rangle - |-,+\rangle}{\sqrt{2}}\right) + d\left(\frac{|+,-\rangle + |-,+\rangle}{\sqrt{2}}\right) \\
E_3^z &= +\frac{J}{2} + D_1^z + \Delta_2^z; \qquad & |\Psi_3^z\rangle &= -d\left(\frac{|+,-\rangle - |-,+\rangle}{\sqrt{2}}\right) + c\left(\frac{|+,-\rangle + |-,+\rangle}{\sqrt{2}}\right) \\
E_4^z &= -\frac{J}{2} - D_1^z + \Delta_1^z; \qquad & |\Psi_4^z\rangle &= -b|-,-\rangle + a|+,+\rangle
\end{aligned} \tag{14}$$

with $\Delta_1^z = \frac{1}{2}\sqrt{4D_4^2 + (g_{zz}^{\mathrm{A}} + g_{zz}^{\mathrm{B}})^2\beta^2 B_0^2}$, $\Delta_2^z = \frac{1}{2}\sqrt{(2J + D_2 - D_3)^2 + (g_{zz}^{\mathrm{A}} - g_{zz}^{\mathrm{B}})^2\beta^2 B_0^2}$ and $|a|^2 + |b|^2 = 1$, $|c|^2 + |d|^2 = 1$. Coefficients a, b, c and d are given in the appendix.

The EPR spectrum of a pair of dissimilar ions is composed of four lines whose energies and intensities are given in table 2. The energy level diagram and the four allowed transitions (represented by arrows) for the magnetic field B_0 parallel to the pair axis are shown in figure 2(a). Figures 2(b) and (c) show the corresponding schematic EPR spectrum versus the microwave energy and the EPR spectrum versus the magnetic field as experimentally recorded. The EPR spectrum of a pair of dissimilar ions is thus composed of two intense lines and two satellites. The splitting between the two intense lines is $2|-2D_1^z - J - \Delta_2^z|$ and the splitting between a satellite and the nearest strong line is equal to $2|2D_1^z + J|$ (figure 2(b)).

When $\mathbf{B}_0$ is perpendicular to the pair axis, along the x axis for example, H_{pair}^x is written as

$$H_{\mathrm{pair}}^x = \begin{pmatrix}
-\frac{J}{2} - D_1^z & \frac{g_{xx}^{\mathrm{A}} - g_{xx}^{\mathrm{B}}}{2\sqrt{2}}\beta B_0 & \frac{g_{xx}^{\mathrm{A}} + g_{xx}^{\mathrm{B}}}{2\sqrt{2}}\beta B_0 & D_4 \\
\frac{g_{xx}^{\mathrm{A}} - g_{xx}^{\mathrm{B}}}{2\sqrt{2}}\beta B_0 & \frac{3J}{2} + D_2 & 0 & \frac{g_{xx}^{\mathrm{B}} - g_{xx}^{\mathrm{A}}}{2\sqrt{2}}\beta B_0 \\
\frac{g_{xx}^{\mathrm{A}} + g_{xx}^{\mathrm{B}}}{2\sqrt{2}}\beta B_0 & 0 & -\frac{J}{2} + D_3 & \frac{g_{xx}^{\mathrm{A}} + g_{xx}^{\mathrm{B}}}{2\sqrt{2}}\beta B_0 \\
D_4 & \frac{g_{xx}^{\mathrm{B}} - g_{xx}^{\mathrm{A}}}{2\sqrt{2}}\beta B_0 & \frac{g_{xx}^{\mathrm{A}} + g_{xx}^{\mathrm{B}}}{2\sqrt{2}}\beta B_0 & -\frac{J}{2} - D_1^z
\end{pmatrix}. \tag{15}$$

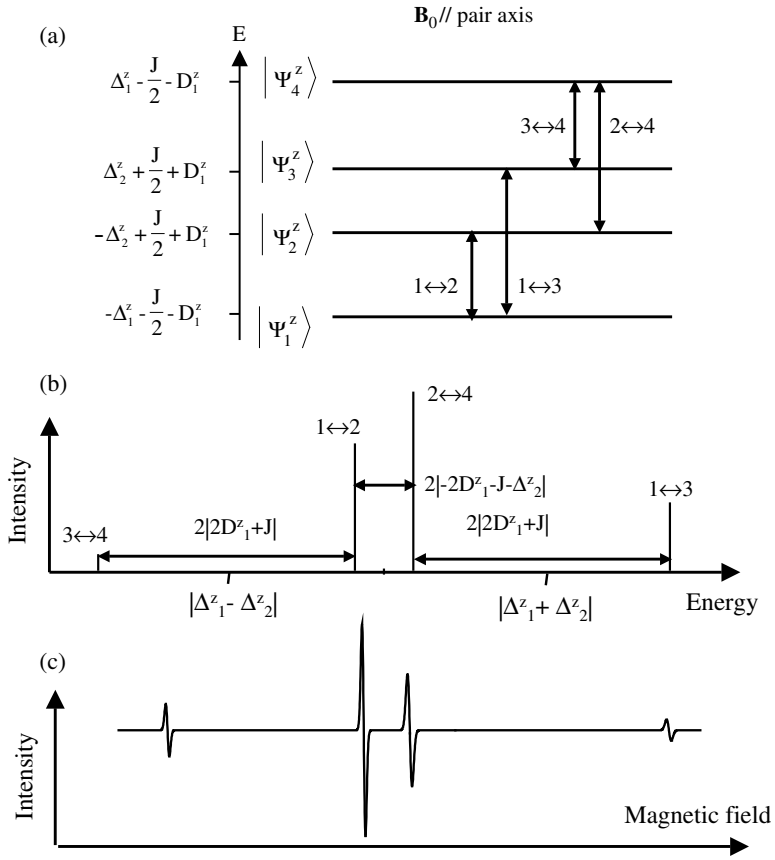

Figure 2. (a) Energy level diagram of a pair of different Kramers ions ($\tilde{g}^{\mathrm{A}} \neq \tilde{g}^{\mathrm{B}}$) for a fixed value of the external magnetic field $\mathbf{B}_0$ parallel to the pair axis and $J > 0$. The g factors are orthorhombic: $g^{\mathrm{A,B}}_{xx} \neq g^{\mathrm{A,B}}_{yy} \neq g^{\mathrm{A,B}}_{zz}$. The four allowed EPR transitions are represented by arrows. (b) Corresponding schematic EPR spectrum as a function of the microwave energy and (c) corresponding EPR spectrum as a function of the magnetic field.

By diagonalization of H^x_{pair}, we obtain the following eigenvalues and eigenvectors:

$$
\begin{aligned}
E^x_1 &= -\frac{J}{2} + \frac{D^x_1}{2} + \Delta^x_1; \qquad |\Psi^x_1\rangle = a'(|-,-\rangle + |+,+\rangle) + b'\left(\frac{|-,+\rangle + |+,-\rangle}{\sqrt{2}}\right)\\
E^x_2 &= -\frac{J}{2} + \frac{D^x_1}{2} - \Delta^x_1; \qquad |\Psi^x_2\rangle = c'(|-,-\rangle + |+,+\rangle) + d'\left(\frac{|-,+\rangle + |+,-\rangle}{\sqrt{2}}\right)\\
E^x_3 &= +\frac{J}{2} - \frac{D^x_1}{2} + \Delta^x_2; \qquad |\Psi^x_3\rangle = \mathrm{e}'(|-,-\rangle - |+,+\rangle) + f'\left(\frac{|+,-\rangle - |-,+\rangle}{\sqrt{2}}\right)\\
E^x_4 &= +\frac{J}{2} - \frac{D^x_1}{2} - \Delta^x_2; \qquad |\Psi^x_4\rangle = g'(|-,-\rangle - |+,+\rangle) + h'\left(\frac{|+,-\rangle - |-,+\rangle}{\sqrt{2}}\right)
\end{aligned}
\tag{16}
$$

with

$$
\begin{aligned}
\Delta^x_1 &= \tfrac{1}{2}\sqrt{(D^z_1 + D_3 - D_4)^2 + (g^{\mathrm{A}}_{xx} + g^{\mathrm{B}}_{xx})^2\beta^2 B^2_0},\\
\Delta^x_2 &= \tfrac{1}{2}\sqrt{(2J + D^z_1 + D_2 + D_4)^2 + (g^{\mathrm{A}}_{xx} - g^{\mathrm{B}}_{xx})^2\beta^2 B^2_0},
\end{aligned}
$$

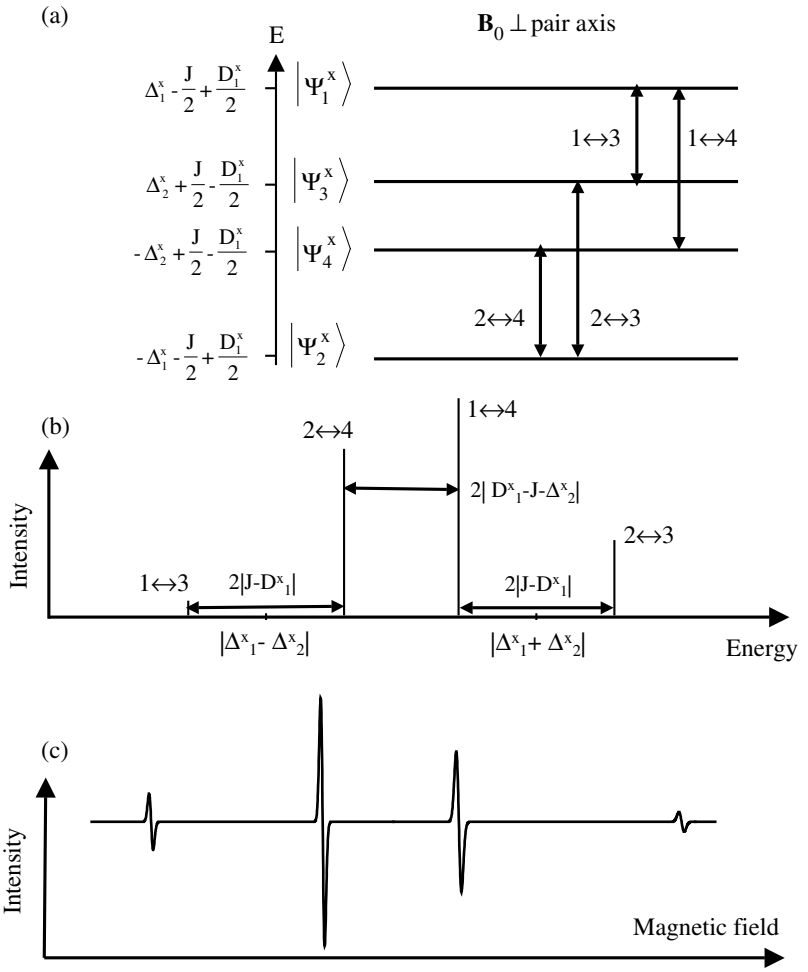

Figure 3. (a) Energy level diagram of a pair of different Kramers ions ($\tilde{g}^{\mathrm{A}} \neq \tilde{g}^{\mathrm{B}}$) for a fixed value of the external magnetic field $\mathbf{B}_0$ perpendicular to the pair axis and $J > 0$. The g factors are orthorhombic: $g^{\mathrm{A,B}}_{xx} \neq g^{\mathrm{A,B}}_{yy} \neq g^{\mathrm{A,B}}_{zz}$. The four allowed EPR transitions are represented by arrows. (b) Corresponding schematic EPR spectrum as a function of the microwave energy and (c) corresponding EPR spectrum as a function of the magnetic field.

$D^x_1 = \frac{\beta^2}{2R^3} g^{\mathrm{A}}_{xx} g^{\mathrm{B}}_{xx}$ and $2|a'|^2+|b'|^2 = 1, 2|c'|^2+|d'|^2 = 1, 2|e'|^2+|f'|^2 = 1$ and $2|g'|^2+|h'|^2 = 1$. Coefficients a', b', c', d', e', f', g' and h' are given in the appendix.

For $\mathbf{B}_0$ perpendicular to the pair axis, four EPR lines are also expected whose energies and intensities are gathered in table 3. The energy level diagram with $\mathbf{B}_0$ perpendicular to the pair axis is shown in figure 3(a) with the four allowed transitions represented by arrows. Figures 3(b) and (c) show the corresponding schematic EPR spectrum versus the microwave energy and versus the magnetic field, respectively. The splitting between the two intense lines is $2|D^x_1 - J - \Delta^x_2|$ and the splitting between a satellite and the nearest strong line is $2|J - D^x_1|$ (figure 3(b)).

By comparing the two orientations $\mathbf{B}_0 \perp$ pair axis and $\mathbf{B}_0 \parallel$ pair axis, it is possible to measure the values of R and J as well as the orientation of the pair in the structure, in contrast to the previous case where only R and the orientation of the pair could be measured.

Table 3. Energies and intensities of the four-line EPR pair spectrum of dissimilar ions with the external magnetic field perpendicular to the pair axis.

Transition	Energy	Intensity proportional to
$E_1^x \rightarrow E_3^x$	$\lvert D_1^x - J + (\Delta_1^x - \Delta_2^x)\rvert$	$[b'f'(g_{zz}^{\mathrm{A}} - g_{zz}^{\mathrm{B}}) - a'e'(g_{zz}^{\mathrm{A}} + g_{zz}^{\mathrm{B}})]^2$
$E_1^x \rightarrow E_4^x$	$\lvert D_1^x - J + (\Delta_1^x + \Delta_2^x)\rvert$	$[b'h'(g_{zz}^{\mathrm{A}} - g_{zz}^{\mathrm{B}}) - a'g'(g_{zz}^{\mathrm{A}} + g_{zz}^{\mathrm{B}})]^2$
$E_2^x \rightarrow E_3^x$	$\lvert -D_1^x + J + (\Delta_1^x + \Delta_2^x)\rvert$	$[d'f'(g_{zz}^{\mathrm{A}} - g_{zz}^{\mathrm{B}}) - e'c'(g_{zz}^{\mathrm{A}} + g_{zz}^{\mathrm{B}})]^2$
$E_4^x \rightarrow E_2^x$	$\lvert -D_1^x + J + (\Delta_1^x - \Delta_2^x)\rvert$	$[d'h'(g_{zz}^{\mathrm{A}} - g_{zz}^{\mathrm{B}}) - c'g'(g_{zz}^{\mathrm{A}} + g_{zz}^{\mathrm{B}})]^2$

3. Experimental EPR pair spectra

We will consider in this section the situations of pairs with similar and dissimilar ions. The case of identical ions is illustrated by neodymium pairs in YVO_4 and $LiYF_4$ hosts and ytterbium pairs in $CsCdBr_3$ [20, 22]. For the first two examples, the pairs are characterized by a strong isotropic exchange interaction measured by high resolution optical spectroscopy and a dipole–dipole magnetic interaction measured by EPR [22]. For the last example, the pairs are characterized by a very small isotropic exchange interaction [20]. The case of pairs of dissimilar ions is illustrated by Nd^{3+} in a $SrAl_{11}O_{19}$ host. In this case, the Nd^{3+} ions of the pair possess different g values and interact via isotropic exchange and dipole–dipole magnetic interactions.

The EPR measurements are performed at 10 K with a X-band Bruker ESP 300e spectrometer equipped with a variable temperature accessory from Oxford Instruments. The crystals are mounted on a small Perspex sample holder to allow their orientation with respect to the magnetic field. The microwave frequency is measured with a Systron Donner frequency counter.

3.1. Pair spectra of rare earth ions with the same g values

YVO_4 single crystals with 0.58% neodymium concentration and $LiYF_4$ single crystals with 1.2% and 2% neodymium doping levels were grown by the Czochralski method. In the zircon-type matrix YVO_4 and the scheelite-type matrix $LiYF_4$, Nd^{3+} ions substitute Y^{3+} ions in a D_{2d} and S_4 point site symmetry, respectively. The free Nd^{3+} ion has a $4f^3$ configuration with a $^{2S+1}L_J = {}^4I_{9/2}$ ground state where S, L and J are the spin, orbital and total momenta, respectively. In a crystal field of S_4, D_{2d} ($LiYF_4$, YVO_4, respectively), the $^4I_{9/2}$ manifold splits into five KDs with only the lowest doublet populated at liquid helium temperature. Neodymium has three even isotopes, ^{142}Nd, ^{144}Nd and ^{146}Nd, with nuclear spins $I = 0$ and a total natural abundance of 79.5%, and two odd isotopes, ^{143}Nd and ^{145}Nd, with nuclear spins $I = 7/2$ and natural abundances of 12.2% and 8.3%, respectively. The EPR spectrum of Nd^{3+} ions is composed of an intense central line due to the even isotopes and a hyperfine pattern of two sets of $2I + 1 = 8$ lines for the two odd isotopes with relative intensities proportional to their natural abundances. In the following we will focus on the central line and we will analyse only the $^{\mathrm{even}}$Nd–$^{\mathrm{even}}$Nd pairs. The following results have already been published in more detail in [22]. Nd:YVO_4 and Nd:$LiYF_4$ crystals correspond to the case of symmetrical pairs with isotropic exchange interaction much larger than the magnetic dipole–dipole interaction. Figures 4(a) and (b) show the π polarized emission spectra of 2% Nd:$LiYF_4$ and 0.58% Nd:YVO_4 samples at 22 and 10 K, respectively, in the vicinity of the $^4F_{3/2} \rightarrow {}^4I_{9/2}$ transitions. For both samples, a complex satellite structure is observed around the $^4F_{3/2} \rightarrow {}^4I_{9/2}$ transitions of isolated Nd^{3+} ions. This structure corresponds to several ferromagnetically coupled pairs with $J_1 = 0.8$ cm^{-1} and $J_2 = 1.6$ cm^{-1} for Nd:$LiYF_4$ (figure 4(a)) and

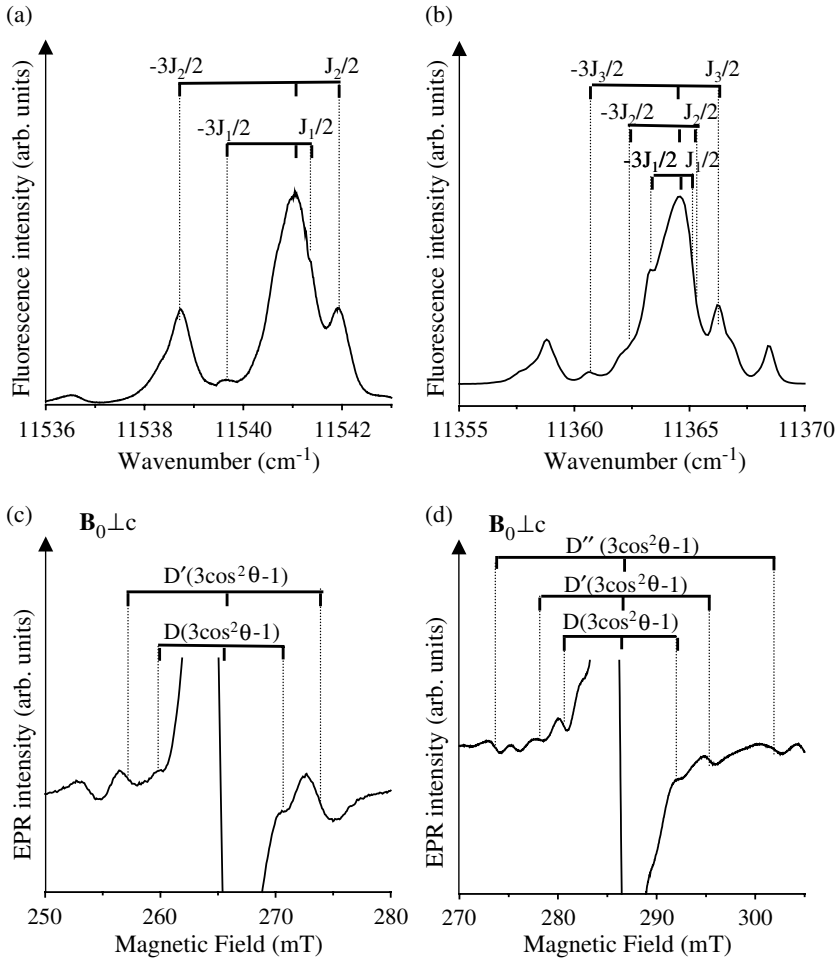

Figure 4. Expanded views of the π polarized $^4F_{3/2} \rightarrow {}^4I_{9/2}$ transitions in (a) 2% Nd:$LiYF_4$ and in (b) 0.58% Nd:YVO_4 crystals. The satellite lines corresponding to ferromagnetically coupled pairs of Nd^{3+} ions are indicated by discontinuous lines. For Nd:$LiYF_4$, two pair lines with $J_1 = 0.8\ cm^{-1}$ and $J_2 = 1.6\ cm^{-1}$ are indicated. For Nd:YVO_4, three pair lines with $J_1 = 0.8\ cm^{-1}$, $J_2 = 1.6\ cm^{-1}$ and $J_3 = 2.7\ cm^{-1}$ are indicated. The central part of the EPR spectrum at 10 K with $\mathbf{B}_0 \perp c$ of (c) 1.2% Nd:$LiYF_4$ and (d) 0.58% Nd:YVO_4. As the Nd–Nd pairs are not oriented along a crystallographic axis, the magnetic dipole–dipole splitting is represented by a term $D(3\cos^2\theta - 1)$ where θ is the angle between $\mathbf{B}_0$ and the pair axis.

$J_1 = 0.8\ cm^{-1}$, $J_2 = 1.6\ cm^{-1}$ and $J_3 = 2.7\ cm^{-1}$ for Nd:YVO_4 (figure 4(b)). This structure is independent of the laser polarization which means that the exchange interaction measured in optical spectroscopy is isotropic. The measurement of the isotropic exchange interaction was possible because this interaction is larger than the resolution of the optical spectroscopy. The EPR spectra gathered in figures 4(c) and (d) for Nd:$LiYF_4$ and Nd:YVO_4, respectively, give direct access to the magnetic dipole–dipole interaction. The central EPR line of figures 4(c) and (d) is due to isolated Nd^{3+} ions located at the Y^{3+} sites. Beside the main EPR signals of isolated ions, several pairs of satellites appear on each side of the central line. These extra lines do not correspond to hyperfine transitions and are due to $^{even}Nd^{3+}$–$^{even}Nd^{3+}$ pairs. The doublet structure observed for the pairs indicates that the two ions are identical with the same g value

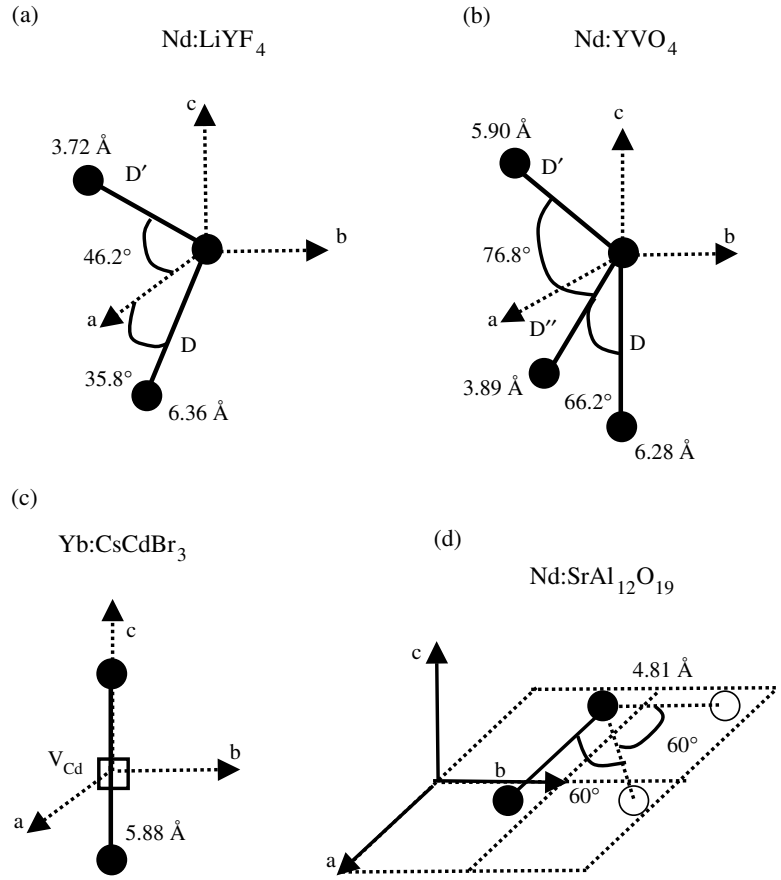

Figure 5. Representation of the crystallographic orientation of the pairs in (a) Nd:$LiYF_4$, (b) Nd:YVO_4, (c) Yb:$CsCdBr_3$ and (d) Nd:$SrAl_{12}O_{19}$. In $LiYF_4$ and YVO_4, the pairs are not oriented along the crystallographic axis. For $CsCdBr_3$, the Yb–Yb pairs are along the c axis and the Cd^{2+} vacancy is represented by a square. For $SrAl_{12}O_{19}$, the pairs are in the (a, b) plane. The three possibilities of pairs with a misorientation of 60° are represented.

(see section 2.1). For both matrices, the line doublets in figures 4(c) and (d) are symmetrically placed around the central line irrespective of the orientation of the magnetic field with respect to the crystallographic axes. This indicates that paired neodymium ions have the same axial g tensor as the isolated neodymium ions, $|g_{\parallel}| = 1.986 \pm 0.003$ and $|g_{\perp}| = 2.553 \pm 0.002$ for Nd:$LiYF_4$ and $|g_{\parallel}| = 0.915 \pm 0.004$ and $|g_{\perp}| = 2.361 \pm 0.003$ for Nd:YVO_4.

As the Y–Y directions in these two hosts are not oriented along the c axis of the structure, the splitting between the line doublets is $D(3\cos^2\theta - 1)$ (figures 4(c) and (d)) where θ is the angle between the magnetic field $\mathbf{B}_0$ and the pair axis. We find zero-field splittings $D = 0.011\,\mathrm{cm}^{-1}$ and $D' = 0.018\,\mathrm{cm}^{-1}$ for Nd:$LiYF_4$ and $D = 0.012\,\mathrm{cm}^{-1}$, $D' = 0.018\,\mathrm{cm}^{-1}$ and $D'' = 0.031\,\mathrm{cm}^{-1}$ for Nd:YVO_4. From the experimental dipole–dipole splitting values, the orientation of the pair axis with respect to the crystallographic axes and the distance R between the two interacting ions can be determined. These results are gathered in figures 5(a) and (b) for Nd:$LiYF_4$ and for Nd:YVO_4, respectively. For Nd:$LiYF_4$ (figure 5(a)), the pairs characterized by the D and D' zero-field splittings are due to pairs oriented at 35.8° from the a axis with $R = 6.36$ Å and to pairs oriented at 46.2° from the a axis with $R = 3.72$ Å, respectively. For

Nd:YVO_4, the D, D' and D'' splittings are due to pairs along the c axis with $R = 6.28$ Å, to pairs oriented at 76.8° from D'' pairs with $R = 5.90$ Å and to pairs oriented at 66.2° from the c axis with $R = 3.89$ Å. The very good agreement between the experimental orientation and Nd–Nd distances and the crystallographic Y–Y orientations and distances in Nd:$LiYF_4$ and Nd:YVO_4 confirms that only the magnetic dipole–dipole interaction is responsible for the doublet splitting. As the isotropic exchange interaction and the dipole–dipole interaction are determined using two different spectroscopies, a deeper investigation of the nature of the exchange interactions has to be done to correlate the ferromagnetically coupled pairs observed by fluorescence to the magnetic dipolar coupled pairs observed by EPR. This study is not the purpose of the present work.

$CsCdBr_3$ single crystals with 1.3% ytterbium concentration were grown by the Bridgman method. A well known feature of $CsCdBr_3$ is that rare-earth ions such as Yb^{3+}, even at low dopant concentration, enter nearly exclusively as charge compensated ion-pair centres in the Cd^{2+} lattice position [19, 20]. The main rare earth centre is a symmetric in-chain Yb^{3+}–V_{Cd}–Yb^{3+} pair complex, where V_{Cd} means a Cd^{2+} vacancy, oriented along the c axis. The free Yb^{3+} ion has a $4f^{13}$ configuration. The ground state is $^2F_{7/2}$ and the $^2F_{5/2}$ excited state is around 10 000 cm^{-1}. In a trigonal field of C_{3v} symmetry (Cd^{2+} site in $CsCdBr_3$), the $J = 7/2$ level splits into four KDs. In addition to even isotopes (nuclear spin $I = 0$), ytterbium has two odd isotopes which give rise to hyperfine structure, ^{171}Yb with nuclear spin $I = 1/2$ (natural abundance 14.4%) and ^{173}Yb with nuclear spin $I = 5/2$ (natural abundance 16.6%). As in the case of neodymium ions, we focus on the central line and analyse only the ^{even}Yb–^{even}Yb pairs. The complete analysis has been published in [20].

The Yb:$CsCdBr_3$ host corresponds to the case of a pair of identical ions with a very small isotropic exchange interaction which has been determined from the hyperfine structure and to a dipole–dipole magnetic interaction [20]. Part of the EPR signal of ytterbium ions in $CsCdBr_3$ is shown in figure 6 for the external magnetic field $\mathbf{B}_0$ parallel to the pair axis (figure 6(a)) and perpendicular to the pair axis (figure 6(b)). The complexity of the spectra is due to the fact that ytterbium has one even isotope of natural abundance 69% and two odd isotopes which are responsible for the hyperfine structure. All the spectral features can be accurately described by assigning the resonance lines to the symmetric pairs of identical ions of the type ^{even}Yb–V_{Cd}–^{even}Yb, ^{171}Yb–V_{Cd} –^{even} Yb and ^{173}Yb–V_{Cd}–^{even}Yb [20]. In the following we will focus on the two central lines due to ^{even}Yb–V_{Cd}–^{even}Yb pairs. The doublet structure of the central line indicates that the two Yb^{3+} ions are identical with the same g values. As the splitting with the field parallel to the pair axis (figure 6(a)) is twice the splitting with the field perpendicular to the pair axis, this implies that $D_4 = 0$. Thus $g_{xx} = g_{yy}$ and the ytterbium site symmetry cannot be lower than axial. The simulations gives an axial g tensor: $|g_\parallel| = 2.503 \pm 0.001$ and $|g_\perp| = 2.619 \pm 0.001$. The magnetic dipolar interaction $D = \frac{\beta^2}{2R^3}(2g_\parallel^2 + g_\perp^2) = 0.043$ cm^{-1} between the two main lines gives an interionic distance R of 5.88 Å which indicates a significant relaxation of 12% of Yb^{3+} ions towards the Cd^{2+} vacancy along the c axis which is the Yb–V_{Cd}–Yb axis (figure 5(c)).

As we have seen previously, when the two ions of the pair are identical, the EPR spectrum does not permit us to estimate the isotropic exchange interaction, unless the rare earth ions possess a hyperfine structure [36]. Indeed, if the hyperfine term is not too small compared to the singlet–triplet splitting J, there is an admixture of the $|\varphi_2\rangle = \frac{1}{\sqrt{2}}(|+,-\rangle - |-,+\rangle)$ singlet state with the $|\varphi_3\rangle = \frac{1}{\sqrt{2}}(|+,-\rangle + |-,+\rangle)$ triplet state. The hyperfine splittings become dependent on J and transitions between singlet and triplet states are no longer strictly forbidden [36]. In $CsCdBr_3$, the value of $J = -0.0016$ cm^{-1} implies that the exchange coupling between the two Yb^{3+} ions is antiferromagnetic and extremely weak [20].

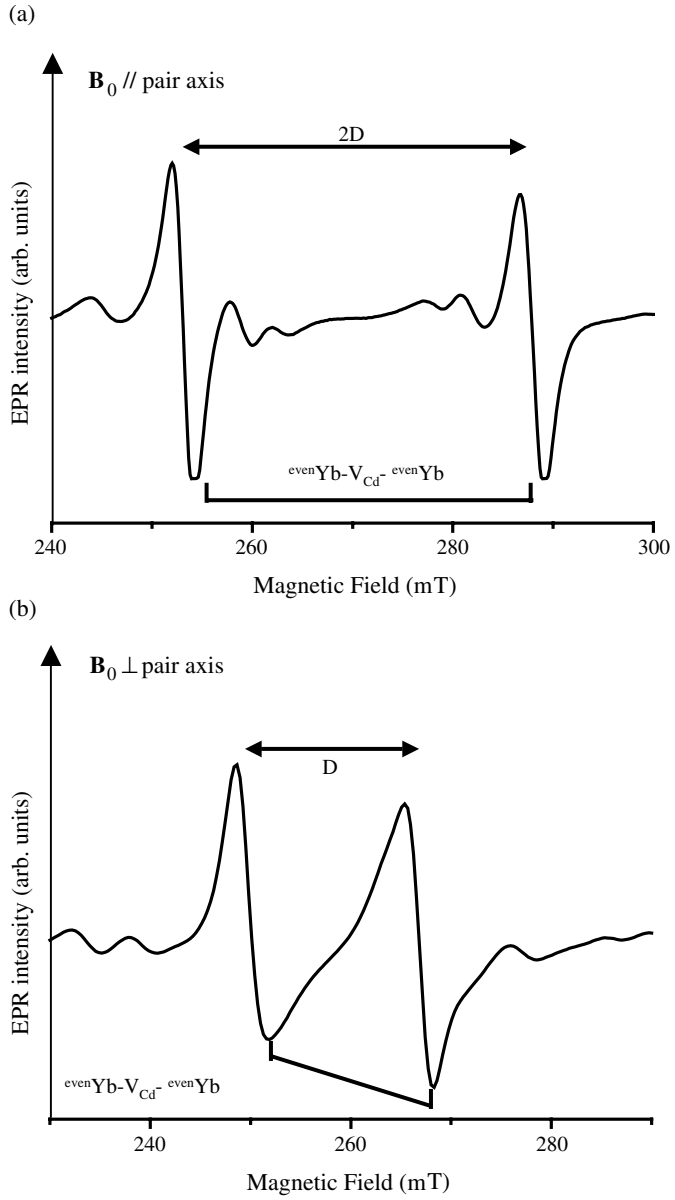

Figure 6. Expanded view of the EPR spectrum of Yb:$CsCdBr_3$ at 10 K with the external magnetic field B_0 (a) parallel to the pair axis (parallel to the crystallographic c axis) and (b) perpendicular to the pair axis (perpendicular to c). The magnetic dipole–dipole splitting is represented.

3.2. Pair spectra of rare earth ions with different g values

The $SrAl_{12}O_{19}$ host belongs to the hexagonal magnetoplumbite structure type with space group $P6_3/mmc$ [37]. The rare earth ions substitute the Sr^{2+} ions, which requires charge compensation brought about by the substitution of Mg^{2+} ions for Al^{3+} ions in the spinel blocks of the structure. The nearest neighbour Sr^{2+}–Sr^{2+} distance is equal to 5.562 Å. From a structure refinement performed on the $CaAl_{12}O_{19}$ host, a disordered distribution of the rare earth ions

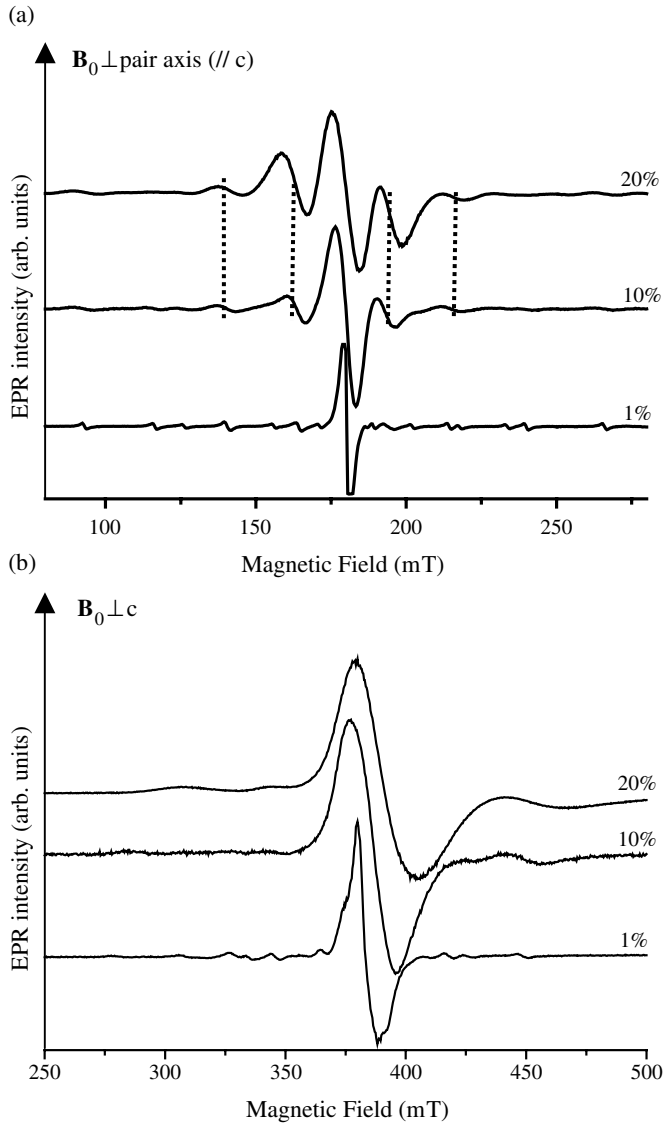

Figure 7. EPR spectra of Nd:$SrAl_{11}O_{19}$ at 10 K for three Nd concentrations 1%, 10% and 20%, recorded with the external magnetic field B_0 (a) perpendicular to the pair axis (parallel to the c axis) and (b) perpendicular to the c axis. The satellites due to Nd pairs are indicated by discontinuous lines.

in the (a, b) mirror plane of the structure is deduced. The neodymium ions can occupy the ideal D_{3h} position, but also a very close position with C_{2v} symmetry [37]. Only one site has been determined from structure refinement with a high thermal factor (0.6) for the strontium compounds, which means that the rare earth ions are free to move around this position. Single crystals have been grown by the melting zone technique for various starting compositions $Sr_{1-x}Nd_xMg_xAl_{12}O_{19}$ with $x = 1\%$, 10% and 20%. The corresponding EPR spectra with the external magnetic field $\mathbf{B}_0$ parallel and perpendicular to the c axis are gathered in figures 7(a) and (b). The best resolution is obtained when the external field is parallel to the c axis, with a

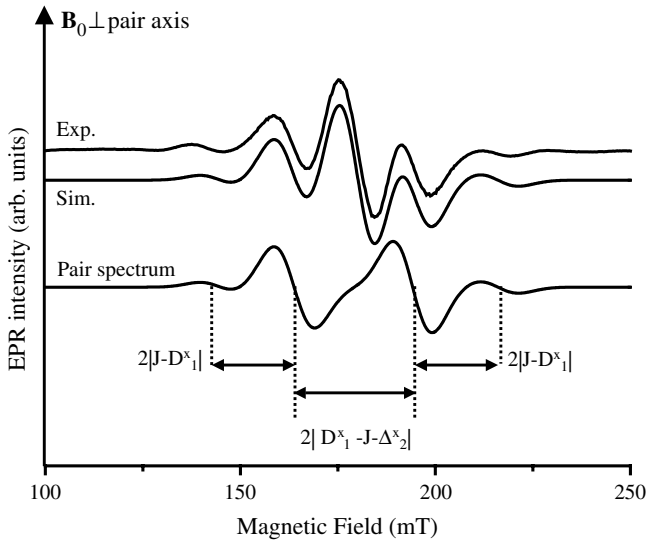

Figure 8. EPR spectra of Nd:$SrAl_{11}O_{19}$ at 10 K for $x = 20\%$ with the external magnetic field B_0 perpendicular to the pair axis (and thus parallel to the c axis). The experimental and simulated spectra are presented as well as the contribution of the pair spectrum.

linewidth of 9 mT for the central line (figure 7(a)). When the magnetic field rotates from the c axis to the direction of the (a, b) plane, the lines move towards higher fields (figure 7(b)) and broaden with a linewidth of 26 mT for the central line. This inhomogeneous broadening indicates that several magnetically inequivalent neodymium ions are located in the (a, b) plane. These ions are magnetically equivalent only when the external field is perpendicular to the (a, b) plane (parallel to the c axis) and become magnetically inequivalent when the field is in the (a, b) plane. In the latter case, the position of the central line exhibits small oscillations with a 60° periodicity that reflects the existence of a threefold symmetry. This behaviour has already been seen for the $CaAl_{12}O_{19}$ host [37]. For low concentration ($x = 1\%$), the EPR spectrum is due to isolated Nd^{3+} ions located at the Sr^{2+} axial site with D_{3h} point symmetry: $|g_\parallel| = 1.726 \pm 0.008$ and $|g_\perp| = 3.75 \pm 0.01$. When the external magnetic field is parallel to the c axis (figure 7(a)) and when the concentration increases from $x = 1$ to 20%, a four-line satellite structure, whose intensity increases with neodymium concentration, appears around the central line. These satellites are also seen for the external field perpendicular to the c axis but the EPR lines are too broad to give a very well defined structure. This concentration dependent four-line structure is characteristic of a pair of neodymium ions with different g values as shown in section 2.2. The simulation of the central part of the EPR spectrum corresponding to ^{even}Nd–^{even}Nd pairs with B_0 perpendicular to the c axis is presented in figure 8. The contribution of the pair spectrum is also presented. The simulation is performed by a complete diagonalization of the Hamiltonian of equation (13). The four-line structure is simulated by considering that the two ions involved in the pairs are characterized by different values of axial g factors with the same orientation: $g_\parallel^A = 1.7 \pm 0.1$, $g_\perp^A = 3.915 \pm 0.02$ and $g_\parallel^B = 1.7 \pm 0.1$, $g_\perp^B = 3.634 \pm 0.03$ with the g_z tensor axis parallel to the Nd–Nd axis The interaction between the two ions is due to an isotropic exchange interaction $J = -0.018 \pm 0.001\ cm^{-1}$ and to a magnetic dipole–dipole contribution which gives a Nd–Nd distance of 4.8 Å corresponding to a relaxation of about 14% compared to the Sr^{2+}–Sr^{2+} distances. This strong relaxation could be due to the fact that the rare earth ions are free to move in the (a, b) plane around the Sr^{2+} position. The positions

of the lines as well as their intensities are well reproduced by the simulation, with only 1% error for the two external satellites at 142.6 and 215 mT and only 0.1% error in the position for the two main lines at 163.8 and 194.9 mT. The small discrepancies observed between the experimental and simulated spectrum could be explained by a small distortion of the axial g tensor giving rise to an orthorhombic tensor and/or the fact that we only consider an isotropic exchange interaction. To our knowledge, this is only the second example encountered in the literature of a pair of Kramers ions with different ground state g-factor values. In [29], a pair of two interacting dissimilar Dy^{3+} ions have been observed in lanthanide nicotinate dihydrate. In [11], Clemens and Hutchison have obtained an EPR spectrum of different neodymium ions in $LaCl_3$. However, in this work, one of the two ions of the pair was pumped in a photoexcited state characterized by a different g factor compared to the KD ground state.

It is important to remark that the four-line spectrum appears in the $SrAl_{12}O_{19}$ host for only small g-factor differences: $g_\perp^A = 3.915$ and $g_\perp^B = 3.634$. In [38], we have studied the influence of crystal field differences between the two ions on the shape of the pair spectrum. Even for very small differences of g factors, the spectrum can exhibit the four-line pattern, as is the case for neodymium pairs in $SrAl_{12}O_{19}$.

By considering the parameters of the simulation obtained for the field orientation parallel to the c axis, it is possible to simulate the pair spectrum when the field is in the (a, b) plane (figure 9). The three possible pair spectra (with an orientation of 60° from each other, see figure 5(d)) are represented by squares, open circles and triangles in figure 9. As the angle θ between the magnetic field and the pair axis is not known, the angular variations of the three four-line pair spectra are calculated for θ varying between 0° and 180°. The simulation gives a range of positions for each line of the pair spectrum (arrows in figure 9) which is in agreement with the linewidth of the experimental four-line pair spectrum.

4. Conclusion

We have revisited in this paper the problem of the electron paramagnetic resonance of rare earth ion pairs. In the case of identical ions with the same g values and a very general g tensor, the EPR pair spectrum is the usual doublet of transitions. The splitting between the two lines as a function of the orientation of the external constant magnetic field gives the interionic distance and the orientation of the pair in the structure. However the isotropic exchange interaction J cannot be measured from the doublet pattern. In YVO_4 and $LiYF_4$ matrices for example, at least two and three pairs of identical neodymium ions have been identified, respectively. These pairs are characterized by strong ferromagnetic isotropic exchange interactions that have been measured directly by optical spectroscopy. In the $CsCdBr_3$ host, more than 95% of the ytterbium ions form weakly antiferromagnetic coupled symmetric Yb^{3+}–V_{Cd}–Yb^{3+} pair complexes of identical ytterbium pairs. In this case, J was measured from the hyperfine splitting pattern of the EPR spectrum.

In the case of dissimilar ions (different ions or identical ions feeling different crystal fields), the pair EPR spectrum is composed of four lines. The splitting between these lines as a function of the orientation of the magnetic field gives a direct measurement of the dipole–dipole interaction term as well as the isotropic exchange interaction. This four-line signature is well identified for pairs of neodymium ions in the $SrAl_{12}O_{19}$ host. The two paired ions are characterized by slightly different axial g-factor values: $g_\perp^A = 3.915 \pm 0.02$ and $g_\perp^B = 3.634 \pm 0.03$. The isotropic exchange interaction $J = -0.018 \pm 0.001\ cm^{-1}$ is measured from the four-line pattern. It is important to note that the additional satellites could have been omitted in the interpretation of many EPR spectra of rare earth ion pairs in the literature or wrongly interpreted as due to impurities or minority pair spectra characterized by short ion–ion distances (large splitting).

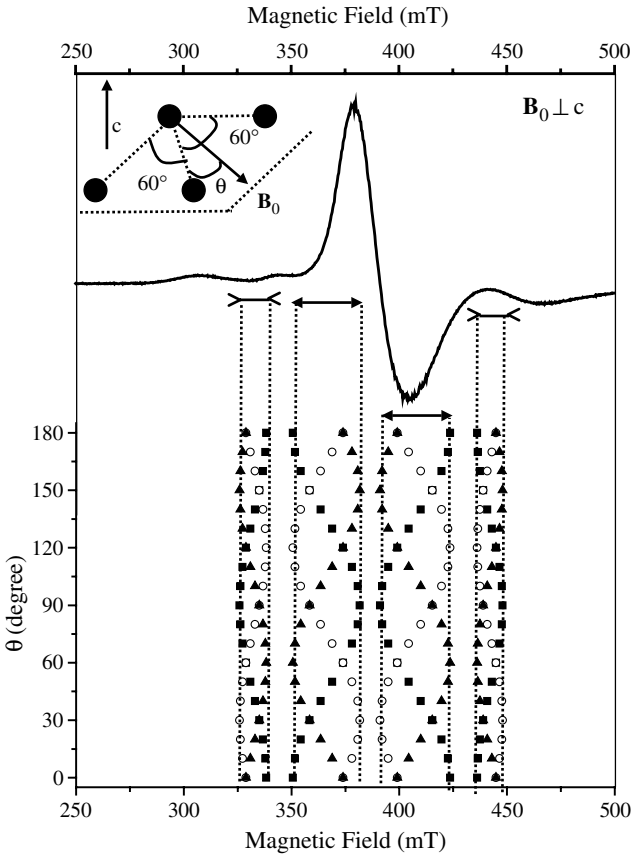

Figure 9. EPR spectrum of Nd:$SrAl_{11}O_{19}$ at 10 K for $x = 20\%$ with the external magnetic field B_0 perpendicular to the c axis. θ is the angle between the external magnetic field and the pair axis. In this plane, the three possible pair spectra which correspond to three pairs misoriented by 60° are represented by squares, open circles and up triangles. These three pairs are not magnetically equivalent when $\mathbf{B}_0$ is in the (a, b) plane. As the angle θ is not known, the angular variations of the three four-line pair spectra are gathered for θ varying between 0 and 180°. This gives a range of positions for each line (inhomogeneous linewidth) of the pair spectrum represented by arrows on the figure.

Appendix. Coefficients of the wavefunctions

A.1. Pairs of ions with the same g values

When the external magnetic field $\mathbf{B}_0$ is parallel to the pair axis, the coefficients of the wavefunctions $|\Psi_1^z\rangle = \alpha|-,-\rangle + \beta|+,+\rangle$ and $|\Psi_4^z\rangle = -\beta|-,-\rangle + \alpha|+,+\rangle$ are

$$\alpha = -\frac{g_{zz}\beta B_0 + \Delta}{\sqrt{(g_{zz}\beta B_0 + \Delta)^2 + D_4^2}}$$
$$\beta = \frac{D_4}{\sqrt{(g_{zz}\beta B_0 + \Delta)^2 + D_4^2}} \tag{A.1}$$

with $\Delta = \sqrt{D_4^2 + g_{zz}^2\beta^2 B_0^2}$.

When the external magnetic field $\mathbf{B}_0$ is perpendicular to the pair axis, the coefficients of the wavefunctions $|\Psi_1^x\rangle = \alpha'(|-,-\rangle+|+,+\rangle)+\beta'(\frac{|-,+\rangle+|+,-\rangle}{\sqrt{2}})$ and $|\Psi_2^x\rangle = \gamma'(|-,-\rangle+|+,+\rangle)+\delta'(\frac{|-,+\rangle+|+,-\rangle}{\sqrt{2}})$ are given by

$$\begin{aligned}
\alpha' &= \frac{\sqrt{2}g_{xx}\beta B_0}{\sqrt{(D_1^z + D_3 - D_4 + 2\Delta')^2 + 4g_{xx}^2\beta^2 B_0^2}} \\
\beta' &= -\frac{D_1^z + D_3 - D_4 + 2\Delta'}{\sqrt{(D_1^z + D_3 - D_4 + 2\Delta')^2 + 4g_{xx}^2\beta^2 B_0^2}} \\
\gamma' &= \frac{\sqrt{2}g_{xx}\beta B_0}{\sqrt{(D_1^z + D_3 - D_4 - 2\Delta')^2 + 4g_{xx}^2\beta^2 B_0^2}} \\
\delta' &= \frac{D_1^z + D_3 - D_4 - 2\Delta'}{\sqrt{(D_1^z + D_3 - D_4 - 2\Delta')^2 + 4g_{xx}^2\beta^2 B_0^2}}
\end{aligned} \tag{A.2}$$

with $\Delta' = \frac{1}{2}\sqrt{(D_1^z - D_4 + D_3)^2 + 4g_{xx}^2\beta^2 B_0^2}$.

A.2. Pairs of ions with different g values

When the external magnetic field $\mathbf{B}_0$ is parallel to the pair axis, the coefficients of the wavefunctions $|\Psi_1^z\rangle = a|-,-\rangle + b|+,+\rangle$ and $|\Psi_2^z\rangle = c(\frac{|+,-\rangle-|-,+\rangle}{\sqrt{2}}) + d(\frac{|+,-\rangle+|-,+\rangle}{\sqrt{2}})$ are

$$\begin{aligned}
a &= -\frac{\frac{(g_{zz}^{\mathrm{A}}+g_{zz}^{\mathrm{B}})}{2}\beta B_0 + D_1^z}{\sqrt{\left[\frac{(g_{zz}^{\mathrm{A}}+g_{zz}^{\mathrm{B}})}{2}\beta B_0 + \Delta_1^z\right]^2 + D_4^2}} \\
b &= \frac{D_4}{\sqrt{\left[\frac{(g_{zz}^{\mathrm{A}}+g_{zz}^{\mathrm{B}})}{2}\beta B_0 + \Delta_1^z\right]^2 + D_4^2}} \\
c &= \frac{D_3 - D_2 - 2J - 2\Delta_2^z}{\sqrt{(D_3 - D_2 - 2J - 2\Delta_2^z)^2 + (g_{zz}^{\mathrm{B}} - g_{zz}^{\mathrm{A}})^2\beta^2 B_0^2}} \\
d &= \frac{(g_{zz}^{\mathrm{B}} - g_{zz}^{\mathrm{A}})\beta B_0}{\sqrt{(D_3 - D_2 - 2J - 2\Delta_2^z)^2 + (g_{zz}^{\mathrm{B}} - g_{zz}^{\mathrm{A}})^2\beta^2 B_0^2}}
\end{aligned} \tag{A.3}$$

with $\Delta_1^z = \frac{1}{2}\sqrt{4D_4^2 + (g_{zz}^{\mathrm{A}} + g_{zz}^{\mathrm{B}})^2\beta^2 B_0^2}$ and $\Delta_2^z = \frac{1}{2}\sqrt{(2J + D_2 - D_3)^2 + (g_{zz}^{\mathrm{A}} - g_{zz}^{\mathrm{B}})^2\beta^2 B_0^2}$.

When the external magnetic field $\mathbf{B}_0$ is perpendicular to the pair axis, the coefficients of the wavefunctions are written as

$$\begin{aligned}
a' &= \frac{D_4 - D_3 - D_1^z + 2\Delta_1^x}{\sqrt{2(D_4 - D_3 - D_1^z + 2\Delta_1^x)^2 + 2(g_{zz}^{\mathrm{A}} + g_{zz}^{\mathrm{B}})^2\beta^2 B_0^2}} \\
b' &= \frac{\sqrt{2}(g_{zz}^{\mathrm{A}} + g_{zz}^{\mathrm{B}})\beta B_0}{\sqrt{2(D_4 - D_3 - D_1^z + 2\Delta_1^x)^2 + 2(g_{zz}^{\mathrm{A}} + g_{zz}^{\mathrm{B}})^2\beta^2 B_0^2}} \\
c' &= \frac{D_4 - D_3 - D_1^z - 2\Delta_1^x}{\sqrt{2(D_4 - D_3 - D_1^z - 2\Delta_1^x)^2 + 2(g_{zz}^{\mathrm{A}} + g_{zz}^{\mathrm{B}})^2\beta^2 B_0^2}}
\end{aligned}$$

$$
\begin{aligned}
d' &= \frac{\sqrt{2}(g_{zz}^{\mathrm{A}} + g_{zz}^{\mathrm{B}})\beta B_0}{\sqrt{2(D_4 - D_3 - D_1^z - 2\Delta_1^x)^2 + 2(g_{zz}^{\mathrm{A}} + g_{zz}^{\mathrm{B}})^2\beta^2 B_0^2}} \\
e' &= \frac{2J + D_1^z + D_2 + D_4 - 2\Delta_2^x}{\sqrt{2(2J + D_1^z + D_2 + D_4 - 2\Delta_2^x)^2 + 2(g_{zz}^{\mathrm{B}} - g_{zz}^{\mathrm{A}})^2\beta^2 B_0^2}} \\
f' &= \frac{\sqrt{2}(g_{zz}^{\mathrm{B}} - g_{zz}^{\mathrm{A}})\beta B_0}{\sqrt{2(2J + D_1^z + D_2 + D_4 - 2\Delta_2^x)^2 + 2(g_{zz}^{\mathrm{B}} - g_{zz}^{\mathrm{A}})^2\beta^2 B_0^2}} \\
g' &= \frac{2J + D_1^z + D_2 + D_4 + 2\Delta_2^x}{\sqrt{2(2J + D_1^z + D_2 + D_4 + 2\Delta_2^x)^2 + 2(g_{zz}^{\mathrm{B}} - g_{zz}^{\mathrm{A}})^2\beta^2 B_0^2}} \\
h' &= \frac{\sqrt{2}(g_{zz}^{\mathrm{B}} - g_{zz}^{\mathrm{A}})\beta B_0}{\sqrt{2(2J + D_1^z + D_2 + D_4 + 2\Delta_2^x)^2 + 2(g_{zz}^{\mathrm{B}} - g_{zz}^{\mathrm{A}})^2\beta^2 B_0^2}}
\end{aligned}
\tag{A.4}
$$

with

$$
\begin{aligned}
\Delta_1^x &= \tfrac{1}{2}\sqrt{(D_1^z + D_3 - D_4)^2 + (g_{xx}^{\mathrm{A}} + g_{xx}^{\mathrm{B}})^2\beta^2 B_0^2}, \\
\Delta_2^x &= \tfrac{1}{2}\sqrt{(2J + D_1^z + D_2 + D_4)^2 + (g_{xx}^{\mathrm{A}} - g_{xx}^{\mathrm{B}})^2\beta^2 B_0^2}.
\end{aligned}
$$

References

[1] Hehlen M P, Güdel H U, Shu Q, Rai J, Rai S and Rand S C 1994 *Phys. Rev. Lett.* **73** 1103
[2] Lüthi S R, Hehlen M P, Riedener T and Güdel H U 1998 *J. Lumin.* **76/77** 447
[3] Hehlen M P, Kuditcher A, Rand S C and Lüthi S R 1999 *Phys. Rev. Lett.* **82** 3050
[4] Guillot-Noël O, Binet L and Gourier D 2002 *Phys. Rev.* B **65** 245101
[5] Ohlsson N, Mohan R K and Kröll S 2002 *Opt. Commun.* **201** 71
[6] Baker J M 1971 *Rep. Prog. Phys.* **34** 109 and references therein
[7] Hutchings M T, Birgeneau R J and Wolf W P 1968 *Phys. Rev.* **168** 1026
[8] Birgeneau R J, Hutchings M T and Wolf W P 1969 *Phys. Rev.* **179** 275
[9] Birgeneau R J, Hutchings M T and Rogers R N 1968 *Phys. Rev.* **175** 1116
[10] Baker J M, Riley J D and Shore R G 1966 *Phys. Rev.* **150** 198
[11] Clemens J M and Hutchison C A Jr 1983 *Phys. Rev.* B **28** 50
[12] Brower K L, Stapleton H J and Brower E O 1966 *Phys. Rev.* **146** 233
[13] McPherson G L and Henling L M 1977 *Phys. Rev.* B **16** 1889
[14] Henling L M and McPherson G L 1977 *Phys. Rev.* B **16** 4756
[15] Dweck J and Seidel G 1966 *Phys. Rev.* **151** 289
[16] Simon F, Rockenbauer A, Fehèr T, Janossy A, Chen C, Chowdhury A J S and Hodby J W 1999 *Phys. Rev.* B **59** 12072
[17] Velter-Stefanescu M, Nistor S V and Grecu V V 1986 *Phys. Rev.* B **34** 1459
[18] Baker J M and Marsh D 1979 *J. Phys. C: Solid State Phys.* **12** 2847
[19] Malkin B Z, Leushin A M, Iskhakova A I, Heber J, Altwein M, Moller K, Fazlizhanov I I and Ulanov V A 2000 *Phys. Rev.* B **62** 7063
[20] Mehta V and Gourier D 2001 *J. Phys.: Condens. Matter* **13** 4567
[21] Kalbfleisch H, Kumberg H, Müller-Vogt G and Stengel M 1972 *Phys. Status Solidi* b **52** 499
[22] Guillot-Noël O, Mehta V, Viana B, Gourier D, Boukhris M and Jandl S 2000 *Phys. Rev.* B **61** 15338
[23] Baker J M 1964 *Phys. Rev.* A **136** 1341
[24] Dweck J and Seidel G 1966 *Phys. Rev.* **146** 359
[25] Baker J M 1964 *Phys. Rev.* A **136** 1633
[26] Dweck J and Seidel G 1967 *Phys. Rev.* **155** 267
[27] Krygin I M, Prokhorov A D, D'yakonov V P, Borowiec M T and Szymczak H 2002 *Phys. Solid State* **44** 1587

[28] Baker J M, Cook M I, Hutchison C A Jr, Leask M J M, Robinson M G, Troncon A L and Wells M R 1991 *Proc. R. Soc.* A **434** 695
[29] Baker J M, Cook M I, Hutchison C A Jr, Martineau P M, Troncon A L and Weber R T 1991 *Proc. R. Soc.* A **434** 707
[30] Hillmer W 1973 *Phys. Status Solidi* b **55** 305
Kingler H, Hillmer W and Kahle H G 1974 *Phys. Status Solidi* b **64** 533
[31] Freeman A J and Watson R E 1962 *Phys. Rev.* **127** 2058
[32] Abragam A and Bleaney B 1970 *Electron Paramagnetic Resonance of Transition Ions* (Oxford: Oxford University Press)
[33] Gafurov M R, Iskhakova A I, Kurkin I N, Kurzin S P, Malkin B Z, Nikitin S I, Orlinskii S B, Rakhmatullin R M, Shakurov G S, Tarasov V F, Demirbilek R and Heber J 2002 *SPIE Proc.* **4766** 279
[34] Tarasov V F, Shakurov G S, Malkin B Z, Iskhakova A I, Heber J and Altwein M 1997 *JETP Lett.* **65** 559
[35] Prinz G A 1966 *Phys. Rev.* **152** 474
[36] Culvahouse J W, Schinke D P and Pfortmiller L G 1969 *Phys. Rev.* **177** 454
[37] Alablanche S, Kahn-Harari A, Thery J, Viana B, Vivien D, Dexpert-Ghys J and Faucher M 1992 *J. Solid State Chem.* **98** 105
[38] Guillot-Noël O, Goldner Ph, Higel P and Gourier D 2003 *Chem. Phys. Lett.* **380** 563